

## The Examination of Corrosion Behaviours of HAP coated Ti Implant Materials and 316L SS by Sol–Gel Method

Aysel BÜYÜKŞAĞI S<sup>a</sup>, Nihal ÇİFTÇİ<sup>a</sup>, Yavuz ERGÜN<sup>b</sup>, and Yusuf KAYALI<sup>c</sup>

<sup>a</sup> Afyonkarahisar Kocatepe University, Science and Art Faculty, Afyonkarahisar, Turkey

<sup>b</sup> Uşak University, Art Faculty, Uşak, Turkey

<sup>c</sup> Afyonkarahisar Kocatepe University, Technical Education Faculty, Afyonkarahisar, Turkey

e-mail: ayselbuyuksagis@hotmail.com, absagis@aku.edu.tr

**Abstract**—In this research, hydroxyapatite (HAP) coatings have been produced on Ti, Ti6Al4V alloy and 316L stainless steel substrates by sol–gel method.  $(\text{NH}_4)_2\text{H}_2\text{PO}_4$  is taken as P precursor and  $\text{Ca}(\text{NO}_3)_2 \cdot 4\text{H}_2\text{O}$  is taken as Ca precursor to obtain HAP coating. Additionally, three different pretreatment processes (HNO<sub>3</sub>, anodic polarization, base-acide (BA)) have been applied to Ti, Ti6Al4V alloy and 316L stainless steel substrates. The corrosion behaviours of bare and HAP coated samples are examined in Ringer and 0.9% NaCl. HAP coated Ti have showed over 87.85% inhibition. HAP coated Ti6Al4V alloys have showed over 87.33% inhibition. In Ringer solution, 99.24% inhibition has been showed in HAP coated anodic pretreatment for 316L stainless steel. All pretreatment processes are effective on clinging of HAP coating to the surface. It is seen that impedance values have increased in HAP coatings (Ti and Ti6Al4V). HAP coatings have raised the corrosion resistance of Ti and Ti6Al4V. The values of polarization resistance in HAP coated samples have increased for 316L stainless steel in 0.9% NaCl and Ringer solutions. It is seen in SEM images that open pores and attachments among pores have been observed in the coating, which increases osteointegration. It is noted in EDX analyses of the surfaces of the HAP coated samples that there is only Ca, O and P on the surface. Ca/P ratio varies in 1.84–2.00 ranges. As Ca/P ratio increases, the inhibition increases too. It is seen in XRD images of HAP powder that there are HA ate structures. Additionally, it is seen in FTIR analysis, characteristic HA absorption bands have occurred in sintered powders.

DOI: 10.1134/S2070205111050054

### INTRODUCTION

The human body contains fluid saturated in both calcium and phosphate ions. Similar concentrations of these ions in a simulated body fluid produced a calcium phosphate layer on the surface of titanium. Metallic implants undergo chemical reactions with ions available in the physiological environment of the human body. Commonly, known as corrosion products, these compounds may accelerate, retard or have no influence on the subsequent deterioration of the metal surface. Unfortunately, many of the most commonly used metal derive little or no protection from the corrosion products that form under normal circumstances. Currently used metallic alloys: austenitic stainless steels, titanium alloys and cobalt chromium alloys, though enjoy superior resistance to corrosion, fail miserably in the harsh environment.

Balamurugan et al. 2006 [1] studied alkoxide based sol–gel technique. Gan and Pilliar (2004a) [2] were prepared sol gel films using either an inorganic precursor solution or an organic precursor solution. The inorganic route–formed film having a lower Ca/P ratio (1.46 cf 2.10 for the organic route–formed film) and having a more irregular topography. Hukovic et al.

2003 [3], electrochemical–corrosion properties of Ti, Ti6Al6Nb and Ti6Al4V implant materials coated with calcium phosphate (CaP) coatings were investigated in vitro in simulated physiological–Hank’s Balanced Salt Solution (HBSS). Well-crystallized HAP and  $\beta$ -TCP exhibited a beneficial corrosion protection effect on the substrate during prolonged exposure to HBSS. Kannan et al. 2003 [4] and Kannan et al. 2004 [5] the corrosion behaviour of various concentrations of sulfuric acid immersion on 316L SS is studied using cyclic anodic polarisation experiments. The results from the experiments showed that 15% and 20% sulfuric acid treated stainless steels showed better with standing to pitting attack compared to the pristine 316L SS. Kannan et al. (2005a) [6], the effect of HNO<sub>3</sub> treatments on 316L SS and the coatings on passivated 316L SS is being explored. The results have indicated that the efficiency of HAP coatings on HNO<sub>3</sub>-treated surface is increased. Kannan et al. (2005b) [7] biphasic ceramic mixtures of different hydroxyapatite and  $\beta$ -tricalciumphosphate ( $\beta$ -TCP) ratios and single phase  $\beta$ -TCP were prepared by a wet chemical process by adjusting the initial Ca/P ratios of the precursors under constant pH and temperature conditions. Increasing calcium deficiency led to a gradual increase in  $\beta$ -TCP content of the mixtures.

<sup>1</sup> The article is published in the original.

Krupa et al. 2001 [8] the corrosion resistance of titanium was examined by electrochemical methods in a simulated body fluid (SBF) at a temperature of 37°C. The results indicate that calcium-ion implantation increases the corrosion resistance. Krupa et al. 2003b [9] the oxidation of titanium in a solution containing calcium and phosphorus ions affects the corrosion resistance and bioactivity of titanium. The examinations have shown that after the oxidation the corrosion resistance increases. Krupa et al. 2005 [10] The corrosion resistance and bioactivity of titanium after sodium-ion implantation were examined. The results obtained indicate that sodium-ion implantation improve the corrosion resistance after short-term exposures. Krupa et al. 2007[11] The corrosion resistance and bioactivity of Ti6Al4V alloy after calcium-ion implantation were examined. The results of the corrosion examinations indicated that under stationary conditions and after short-term exposures, the calcium-ion implanted titanium alloy had an increased corrosion resistance, but during the anodic polarization, calcium-implanted samples underwent pitting corrosion. Xu et al. 2006[12] indicated that the HA phase began to crystallize after a heat treatment at 580°C; and the crystallinity increased obviously at a temperature of 780°C. The HA film showed a porous structure and a thickness of 5–7 µm after the heat treatment at 780°C. Wang et al. 2007 [13] bioactive hydroxyapatite (HA) films were fabricated by a sol–gel method. The results show that all the sol–gel films are composed of the phases of HA, CaO, TiO<sub>2</sub> and CaTiO<sub>3</sub>. With increasing the calcining temperature, the crystallinity of the films increases, the structure becomes more compact and changes from granular and lamellar to cellular structure, and the Ca/P ratio increases slightly because of the loss of P in the films.

## 1. EXPERIMENTAL

Surface condition of the metals play a major role in the development of sol–gel coating and its corrosion resistance. Before dipping into sol, the substrates were polished and then cleaned in an ultrasonic bath of ethanol and acetone. Additionally, three different pre-treatment processes (HNO<sub>3</sub>, anodic polarization, 5 N NaOH–1 N HCl (BA)) have been applied to Ti and Ti6Al4V alloy and 316L stainless steel substrates. Ca(NO<sub>3</sub>)<sub>2</sub> · 4H<sub>2</sub>O is taken as Ca precursor and (NH<sub>4</sub>) · H<sub>2</sub>PO<sub>4</sub> is taken as P precursor to obtain sol [14–18]. Sol was prepared using Ca(NO<sub>3</sub>)<sub>2</sub> · 4H<sub>2</sub>O ethanol solution and (NH<sub>4</sub>) · H<sub>2</sub>PO<sub>4</sub> aqueous solution. These solutions were stirred 70 °C, 4 h. Then they were aged at 24 h. And then (NH<sub>4</sub>) · H<sub>2</sub>PO<sub>4</sub> aqueous solution were added to Ca(NO<sub>3</sub>)<sub>2</sub> · 4H<sub>2</sub>O ethanol solution. %25 NH<sub>4</sub> solution was added for pH settings. sol–gel was vigorously stirred at 70°C, 4 h and was aged 24 h. Ti6Al4V, Ti and 316L stainless steel were coated by

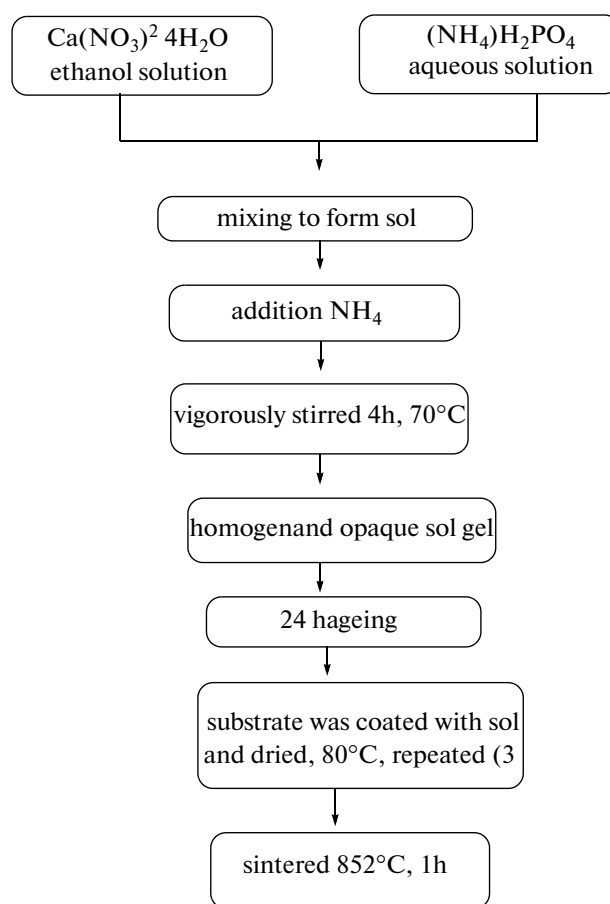


Fig. 1. Flow diagram of sol gel process for preparation of HA film.

using this sol. Flow diagram of sol gel process for preparation of HA films is given Fig. 1.

Coated samples were sintered at 850°C for 1 h and characterised using FTIR, XRD, SEM-EDX studies to confirm its chemical nature and crystallographic structure. Electrochemical studies involving anodic polarization experiments and electrochemical impedance spectroscopy were performed in Ringer's solution (NaCl—8.6 g/L, CaCl<sub>2</sub> · 2H<sub>2</sub>O—0.66 g/L and KCl—0.6 g/L) [4–6] and % 0.9 NaCl solution to assess the corrosion resistance due to surface treatments. Measurements were obtained using a system consisting of a Reference 600 potentiostat/galvanostat ZRA system. Experiments were always repeated at least three times.

## 3. RESULTS AND DISCUSSIONS

### 3.1. SEM-EDX Analyses

The manufacturing of calcium phosphates for biomedical application includes heat treatment of devices for various purposes including sintering of the coating.

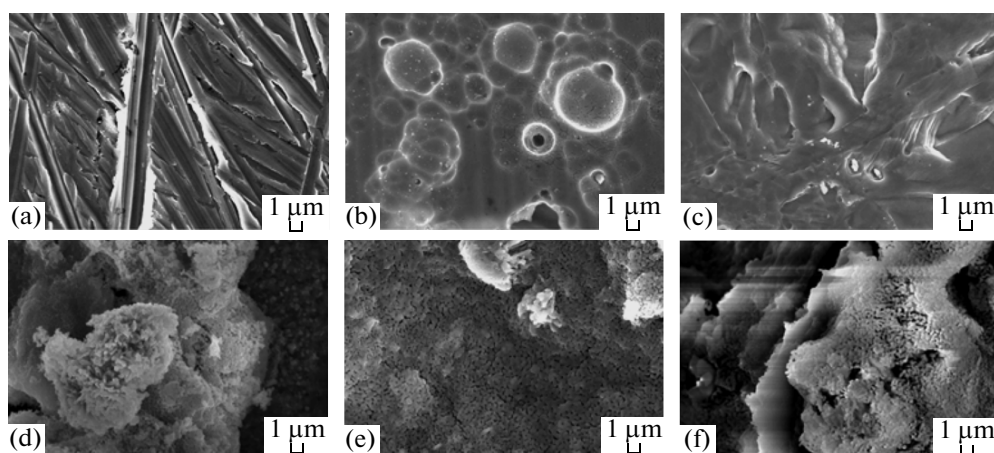
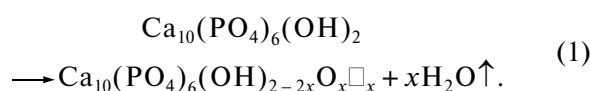


**Fig. 2.** SEM microphotographs of different pretreatments and HAP coated surfaces for 316L stainless (1 μm) (a) HNO<sub>3</sub> pretreatment (b) anodic pretreatment (c) BA pretreatment (d) HAP (HNO<sub>3</sub>) (e) HAP (anodic), (f) HAP (BA).

The knowledge about the thermal behaviour of HAP is important since at high temperatures the HAP structure may be modified [19, 20]. Sintering of HAP in air is complicated by two processes namely dehydroxylation and decomposition of HAP, at elevated temperatures. The dehydroxylation reaction of HAP is given below in Eq. (1) [21],



Where □ is vacancy and  $x < 1$ .

The hydroxyl ion deficient product which is obtained, is known as oxyhydroxyapatite (OHA) [22]. In air OHA is formed at 900°C and in water-free environment it is formed around 850°C. Reversible dehydroxylation generally occurs above 800°C and up to 75–80% of total hydroxyl groups can be lost irreversibly. Sintered HAP coatings were relatively dense and adherent to the substrate. In contrast, HAP coatings for unsintered deposits can be easily removed from the substrates. Because of densification during sintering, shrinkage and cracking of the coatings can occur. Also thermal stress induced by differences in thermal expansion coefficients between metal and the ceramic film during sintering and cooling leads to cracking [23]. Low sintering temperatures can lead to a weakly bonded low density coatings. High sintering temperatures result in degradation of the metal substrate catalysing the decomposition of HAP to anhydrous calcium phosphates. The effect of sintering temperature of HAP coated type 316L SS was studied in air atmosphere from 300 to 900°C for every 100°C for duration of 1 h each. At temperatures lower than 600°C, the adherence of the coatings was very weak and on increasing the sintering time, the properties of the base alloy type 316L SS was affected by sensitization [24].

At over 1050°C, Ti leads to decomposition of HAP and 316L SS at over 950°C causes decomposition of

HAP. Therefore, the sintering temperatures in the present study should be done after keeping at 850°C for 1 hour. The following reaction occurs during sintering [25]:



Ca(NO<sub>3</sub>)<sub>2</sub> · 4H<sub>2</sub>O is taken as calcium precursor and (NH<sub>4</sub>) · H<sub>2</sub>PO<sub>4</sub> is taken as phosphor precursor to obtain sol gel. The important volume changes have occurred in titanium and its alloys at 880 to 960°C temperatures during the transformation of α–β phases. Therefore, the sintering temperatures in Ti and its alloys should be done at 900°C and below of it [24].

The fact that the structure of HAP is very rough and porous morphologically is very important in terms of choosing these areas to use by the cells producing bones. Three different pretreatments are applied the experiment electrodes. These are nitric acid pretreatment (HNO<sub>3</sub>), anodic pretreatment (anodic) and 5 N NaOH–1 N HCl pretreatment (BA). SEM images for 316L steel, HAP coated images after different pretreatments and these pretreatments surfaces are given Fig. 2.

According to Fig. 2 a very homogenous HAP is obtained on the steel which is applied to anodic pretreatment. Steel substrate is scarcely seen and there is little agglomerate in it. When the corrosion of 316L stainless steel in Ringer solution is investigated, it is stated that 99.24% inhibition is also observed in HAP coated anodic pretreatment in Tafel comments. In this stage, 1 N HCl and anodic polarization pretreatment form a barrier layer by forming Fe<sub>2</sub>O<sub>3</sub>, FeO and Cr<sub>2</sub>O<sub>3</sub> oxides on the surface of steel. HAP coatings form an external porous barrier layer. HAP is hydrated in aggressive medium and repairs degraded and broken areas by uniting ions. These effects may be attributed to the rebuild of the barrier layer due to the possible treatments. For Ti HAP coated images after different

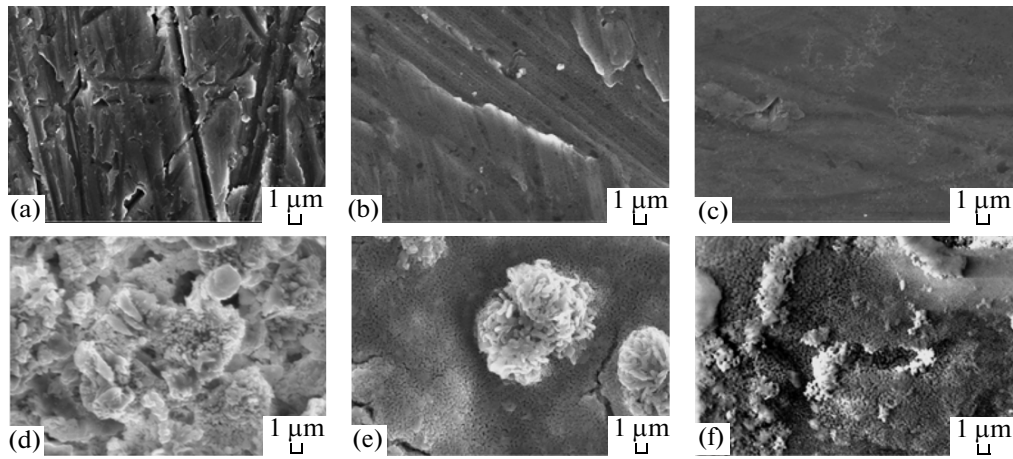


**Fig. 3.** SEM microphotographs of different pretreatments and HAP coated surfaces for Ti (1 μm) (a) HNO<sub>3</sub> pretreatment (b) anodic pretreatment (c) BA pretreatment (d) HAP (HNO<sub>3</sub>) (e) HAP (anodic), (f) HAP(BA).

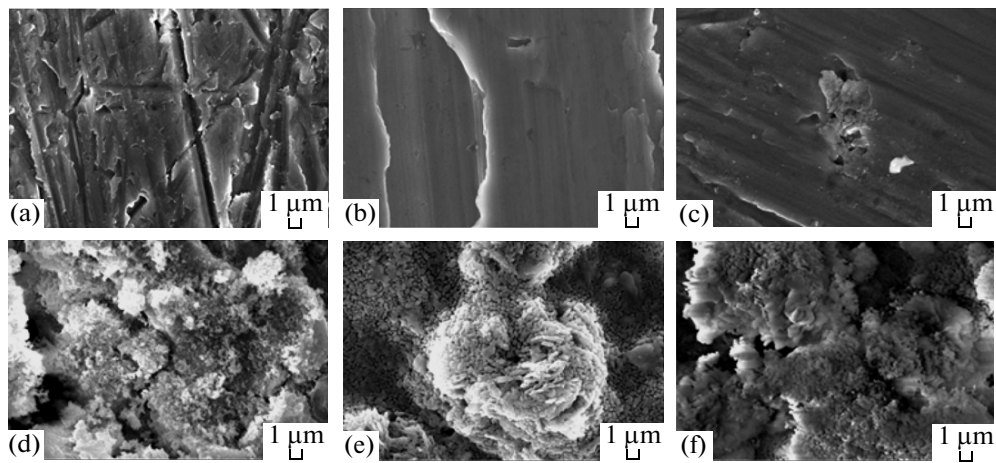


**Fig. 4.** SEM microphotographs of different pretreatments and HAP coated surfaces for Ti6Al4V (1 μm) (a) HNO<sub>3</sub> pretreatment (b) anodic pretreatment (c) BA pretreatment (d) HAP (HNO<sub>3</sub>) (e) HAP (anodic), (f) HAP(BA).

pretreatments and these pretreatments surfaces are given Fig. 3.

According to Fig. 3 the HAP coatings were very porous in nature and drastically increased the surface roughness of the specimens. This, in turn, contributed to a complete change in surface topography. Since the coating is very porous, it is thought that this will allow for the infiltration of cells in vivo which would enhance the dissolution of the Ca–P film and lead to increased rates of positive interaction between the metallic substrate and surrounding hard tissue [26–29]. These effects may be attributed to the rebuild of the barrier layer due to the possible participation.

When Table 2 is examined, % inhibition values are very high. This case can be explained that HA is hydrated and reacts with ions easily and repairs broken film areas easily. The fact that HA is in the form of bars and it has no homogenous structure simplifies osteointegration. HAP coated images for Ti6Al4V

alloy after different pretreatments and these pretreatments surfaces are given Fig. 4.

It is seen in the samples with HNO<sub>3</sub> pretreatment that the surface is roughed grown distinctly. As a result of this, HAP coatings have holding on to the surface well and a homogenous HAP coating has been produced. When HAP coated samples with HNO<sub>3</sub> pretreatment are investigated, it can be said that the surface is completely coated with HAP and there is almost no pore and HAPs are coated in the form of

**Table 1.** EDX quantitative element analyses (% Atom)

	O	P	Ca	Ca/P
HAP (BA) Ti6Al4V alloy	66.25	11.66	22.9	1.96
HAP (BA) 316L SS	66.33	11.87	21.80	1.84
HAP (BA) Pure Ti	45.99	17.90	36.15	2.00

**Table 2.** The corrosion characteristics of Ti

		$-E_{\text{cor}}$ , mV;	$i_{\text{cor}}$ , nAcm <sup>-2</sup>	$R_p$ , k $\Omega$	% inhibition (By use of $i_{\text{cor}}$ )	R1, $\Omega$	W, S $\times$ s <sup>1/2</sup>
Ringer solution	uncoated	120.20	143.00	114.25	–	6.35	$-288.3 \times 10^9$
	HAP coated (HNO <sub>3</sub> )	161.60	9.25	3260.00	93.53	52.16	$-32.69 \times 10^6$
	HAP coated (anodic)	43.76	17.38	2232.00	87.85	246.26	$52.30 \times 10^{-6}$
	HAP coated (BA)	129.00	12.21	2015.00	91.46	58.90	$626.6 \times 10^{-3}$
% 0.9 NaCl solution	uncoated	190.80	211.00	295.00	–	590.75	$770.2 \times 10^6$
	HAP coated (HNO <sub>3</sub> )	160.00	11.80	2698.60	94.40	1222.40	$873.85 \times 10^6$
	HAP coated (anodic)	90.36	6.72	1726.10	96.81	126.20	$107.8 \times 10^{-6}$
	HAP coated (BA)	234.00	4.77	6453.00	97.54	42.57	875.3

Note: – not determined.

agglomerate. It can be observed that the surface in the samples with pretreatment as a very rough structure. This case enables the coating of HAP. Not only coating increases the corrosion resistance, but also it decreases the electrical charge on the metal surface. EDX quantitative element analyses is given Table 1.

It is observed that there is only Ca, O and P in EDX analyses of HAP coated samples' surfaces in Table 1. Calcium phosphate can be classified as groups of a definite Ca/P rate. Hydroxyapatite Ca/P rate is 1.67 [2, 29–32]. Various calcium phosphate rates diversity from 0.5 to 2. Tetracalcium phosphate Ca<sub>4</sub>O(PO<sub>4</sub>)<sub>2</sub> with the highest Ca/P rate is hilgenstockite [33–36]. Calcium phosphate Ca(PO<sub>3</sub>)<sub>2</sub> the lowest Ca/P rate is calcium meta phosphate (CMP). The bioactivity of calcium phosphate depends on the resolution of released Ca<sup>2+</sup> ions which is one of these compounds. If Ca/P rate is 1.5, its structure is tricalcium phosphate (TCP) [33–38]. In the present study Ca/P rates are 1.84 and over of it in EDX analyses. This case shows that HAP occurred on the surface is close hilgenstockie structure [33–38, 4, 29–31].

### 3.2. Electrochemical Studies

This can normally be analyzed using Nyquist diagrams, where the imaginary part of impedance is plotted as a function of real part. The Bode plots show the total impedance  $|Z|$  and phase angle  $\theta$ , as a function of frequency. The corrosion characteristics of Ti are given Table 2.

When the corrosion characteristics for Ti in Ringer solution are examined, it is observed that 87.85% and over inhibition is obtained in HAP coated samples. This case shows that the coatings prevent the corrosion of Ti by coating substantially the entire surface. When % inhibition is investigated, the highest inhibition is in HNO<sub>3</sub> pretreatment and in the samples with pretreatment and it is 93.53%. BA and anodic polarization process follows that. The best pretreatment for Ti in Ringer solution is the process done with HNO<sub>3</sub>. When

$E_{\text{cor}}$  values are examined, it can be observed that they have shifted to more positive values. This case shows that the coatings act as anodic inhibitor. When the corrosion of Ti in 0.9% NaCl is investigated, % inhibition values are very high in HAP coated samples. % inhibition is lower BA compared to HNO<sub>3</sub> and anodic pretreatments. Anodic pretreatment is performed in HCl medium. If there is Cl<sup>-</sup> residuary on the surface as a result of cleaning process, this also causes the decrease of inhibition. When  $E_{\text{cor}}$  values of HAP coated samples are compared to uncoated electrodes has shifted to more positive potentials, except for HAP(BA). HAP coatings also act as anodic inhibitor here. Tafel plots for 316L SS and Ti6Al4V are given Fig. 5. The corrosion characteristics for Ti6Al4V alloy are given in Table 3.

When the corrosion characteristics of Ti6Al4V alloy are examined in Ringer solution, % inhibition values are very high again. The highest inhibition is observed in HAP(BA) coating. The lowest inhibition can be seen in HAP (anodic). All the inhibition values are over 87.33%. This case shows that the alloy surface is coated well and it is protected against corrosion.  $E_{\text{cor}}$  values have shifted to more positive values in all coatings. Coatings act as anodic inhibitor here also. When pretreatments are compared in HAP coated coatings in NaCl medium, BA pretreatment shows higher inhibition. When EIS values of Ti6Al4V (Table 3) are examined, it is seen that pretreatment performed by using NaOH–HCl and HNO<sub>3</sub> are effective on holding of HAP coatings to the surface. There are both porous and barrier layer on Ti alloy in NaCl medium (because of Warburg impedance). The porous layer shows resistance during oxidation. The highest R1 values are observed in HNO<sub>3</sub> pretreatment one. The fact showing similar result to pure Ti shows that HNO<sub>3</sub> forms a more effective protective oxide layer in pre-surface processes. When it contacts with HAP coated sample solution, pores are coated with these occurred oxide productions, which increases the resistance against corrosion.

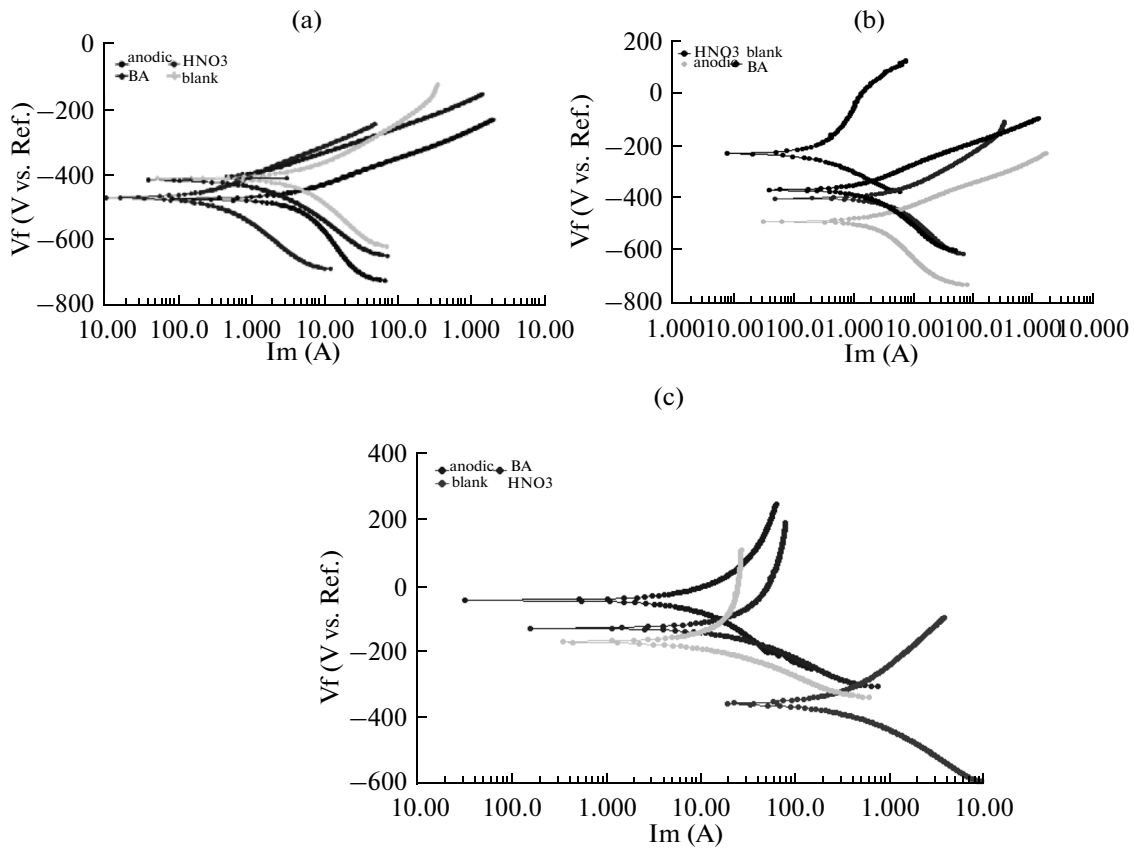


**Fig. 5.** Tafel plots for 316L SS and Ti6Al4V (a) 316L SS in Ringer’s solution (b) 316L SS in % 0.9 NaCl solution (c) Ti6Al4V in % 0.9 NaCl solution.

The interpretation of the results is based upon a two-layer model of the surface film consisting of an inner barrier layer and a thicker porous outer layer. The inner barrier layer dominates the impedance spectra at higher frequencies while the outer layer dominates at low frequencies. The impedance data vary with immersion time, the main variable being an increase in the capacitance and a decrease in the resis-

tance of the inner layer. Since the pores are filled with electrolyte, the contribution from this porous layer to the electrochemical properties is rather small, and the impedance response is dominated by the inner layer which behaves as a non-ideal dielectric with high electronic resistance. The nature of both layers was found to depend on the nature of the electrode substrate material and the presence of phosphate anions.

**Table 3.** The corrosion characteristics for Ti6Al4V alloy

		$-E_{cor}$ , mV	$i_{cor}$ , nAcm <sup>-2</sup>	$R_p$ , k $\Omega$	% inhibition (By use of $i_{cor}$ )	$R_1$ , $\Omega$	$W$ , S $\times$ s <sup>1/2</sup>
Ringer solution	uncoated	299.00	117.00	121.08	—	20.86	$2.0735 \times 10^3$
	HAP coated (HNO <sub>3</sub> )	134.00	11.50	2239.00	90.17	$5.37 \times 10^3$	$345.35 \times 10^6$
	HAP coated (anodic)	33.00	14.82	2561.50	87.33	16.64	$2.143 \times 10^{-6}$
	HAP coated (BA)	115.00	14.33	1652.00	93.95	45.51	1.633
% 0.9 NaCl solution	uncoated	231.30	280.40	98.06	—	20.19	$3.963 \times 10^6$
	HAP coated (HNO <sub>3</sub> )	235.00	28.86	1795.50	89.70	$1.75 \times 10^3$	$447.4 \times 10^6$
	HAP coated (anodic)	164.00	12.98	2200.00	90.69	70.54	$-62.91 \times 10^{-6}$
	HAP coated (BA)	121.50	33.24	1319.00	93.89	39.74	$-4.635 \times 10$

Note: — not determined.

**Table 4.** The corrosion characteristics of 316L stainless steel

		$-E_{cor}$ , mV;	$i_{cor}$ , nAcm <sup>-2</sup>	$R_p$ , k $\Omega$	% inhibition (By use of $i_{cor}$ )	$R_p$ , $\Omega$	Cf, $\mu$ F
Ringer solution	uncoated	188.5	325.54	133.24	—	5.9083	62.323
	HAP coated (HNO <sub>3</sub> )	306	607.64	56.87	-86.66	$28.328 \times 10^3$	153.8
	HAP coated (anodic)	438.5	2.443	4682	99.24	1.081	506.9
	HAP coated (BA)	393.3	1715.92	12.47	-427.1	0.878	113.15
% 0.9 NaCl solution	uncoated	165	343.51	18.14	—	6.774	138.3
	HAP coated (HNO <sub>3</sub> )	387	1229.29	56.24	-258	$230.535 \times 10^3$	$43.04 \times 10^{-6}$
	HAP coated (anodic)	456	1059.9	10.19	-208.5	1.218	0.07
	HAP coated (BA)	371.3	2959.2	13.69	-762.2	8.957	$325.9 \times 10^{-6}$

Note: — not determined.

Pure Ti and Ti6Al4V alloy applied to HNO<sub>3</sub> and pretreatment have high resistance and total impedance value. Oxide film occurred during HNO<sub>3</sub> process is enough to provide passiveness and high resistance. The occurred passive layer increases the decomposition of metal and protects the metal [39]. When the impedance values of pure Ti is examined (Table 2), Warburg impedance (W) is used to model the increasing ionic conductivity because of the corrosion process together with Yo phase element. The highest R1 value of pure Ti is seen in HAP coating with HNO<sub>3</sub> pretreatment in Ringer and 0.9% NaCl solution. This case can be explained that it shows decisive and protective characters against high resistance in NaCl medium. It is observed that HAP occurred on the surface has porous structure in SEM images (Fig. 3). Warburg impedance is related to diffusion process in external porous layer. When the impedance model on Ti is investigated, it is observed that it fits on two layers model [3]. Internal barrier layer is the high frequency area and the external porous layer is the low frequency area. The cycle (devre) model shows that HAP exists

both in porous and barrier layers [9]. The highest R1 values are observed in anodic pretreatment in Ringer physiologic liquid. If the surface of pure Ti stays in the air very much after having brushed, three oxide layers have occurred on its surface. There is the first layer is TiO bond to the metal, Ti<sub>2</sub>O<sub>3</sub> onto it and TiO<sub>2</sub> in outermost. TiO<sub>2</sub> oxide layer contacts with the solution. When Ti is plunged into the solution, the film starts to grow immediately. The increase of corrosion decreases the anodic decomposition of Ti [39]. The corrosion characteristics of 316L stainless steel are given in Table 4.

When 316L SS Ringer solution is investigated, the inhibition is 99.24% in HAP coated anodic pretreatment one. SEM images of HAP coated anodic pretreatment one also confirm this result (Fig. 2e). All of the other inhibitions are negative. This case shows that oxides have occurred on the steel surface of it. The fact that sintering process can not be also done in vacuum medium supports this case. Another pretreatment can be also performed to increase conservation on the surface. In other words, if two pretreatment are applied together, HAP can cling to the surface better. This fact is supported by Olefjord and Elfstrom [40] who proposed that enrichment of alloy elements in the metal phase promotes passivation by lowering the dissolution rate in the active phase preceding passivation. Electrochemical impedance is the complex combination. The electric field enhances the deprotonation of OH<sup>-</sup> ions causing the ingress of protons through the cation selective layer and the ingress of remaining O<sup>2-</sup> anions towards the metal-film interface where reaction with chromium takes place. Due to the fact that Cr<sub>2</sub>O<sub>3</sub> and CrO<sub>3</sub> have very similar standard free enthalpies, it is not surprising that, as postulated by Revesz and Kruger [41] some CrO<sub>3</sub> is formed along with Cr<sub>2</sub>O<sub>3</sub>. Similarly, the surface treatment induced by thus, sintering of the different ceramic coatings on type 316L SS is not effective in producing stoichiometric coatings and effect on passivation have not induced any significant effects while sintering in air

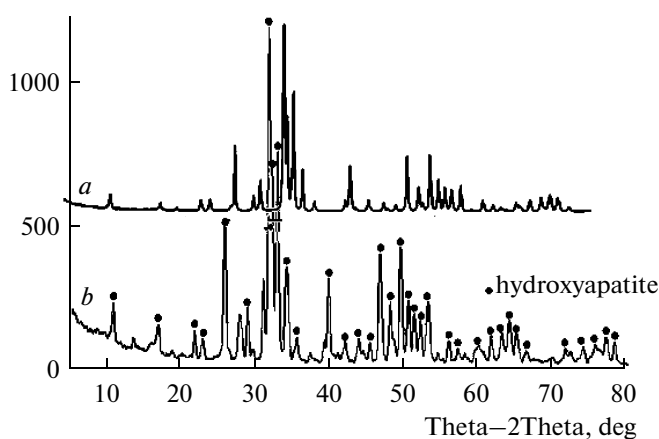


**Fig. 6.** XRD analyses HA powders (a) standart HA peak (b) experimental obtained HA peak at sintered 850°C.

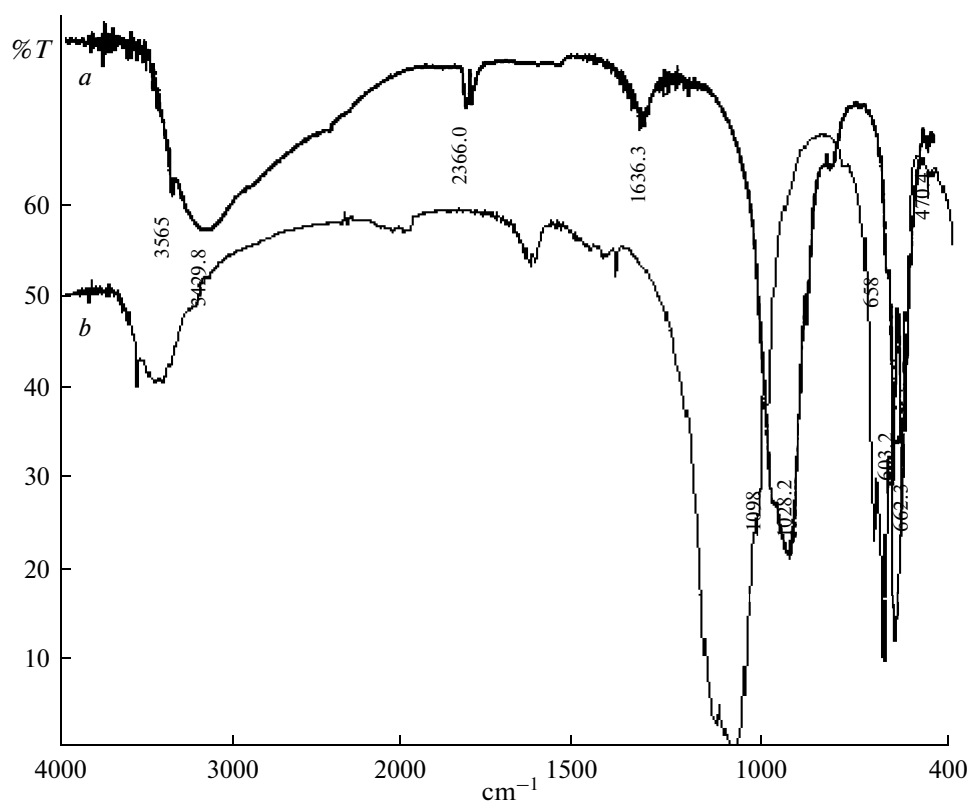


Fig. 7. FTIR spectrum of HA powders at sintered 850°C (a) standart HA peak (b) experimental obtained HA peak.

atmosphere. The obtained values have been showed increase in the corrosion resistivity of the coatings.

According to Table 4 when 316L is investigated, the noble metals simplify existed inside of 316L steel the passivation of the surface.  $\text{Cl}^-$  ions existed in NaCl and Ringer solution attack the surface because of porous structure of HAP coating and they determinate the occurred passive film [5]. Consequently, the film shows less protective character and low corrosion resistance [25]. When it is coated with HAP, its corrosion resistance has increased. HAP coating becomes hydratized and it coats the porous by uniting with ions easily. Coating optimum parameters are observed by decreasing of double layer capacity (Cf) and increasing of resistance.

Not only coating decreases corrosion resistance, but also it reduces the electrical charging on the surface. HAP coating inhibits electrochemical reactions on electrode surface. The reaction productions on the electrode surface prevent mass transfer of oxygen and it increases  $R_p$  by coating electrode surface. Constant phase element ( $Y_o$ ) contributes to double layer capacitance (Cf) of oxide film on the steel surface.  $Y_o$  provides not to have rough and homogenous structure of passive and porous layers. Moreover, it is available in microscobic level under oxide phase and oxide electrolyte interferences, it is necessary due to the distribu-

tion of relaxation times as a result of non-homogenous impurity.

### 3.3 XRD Analyses

It is significant to stress here that the CaP deposition technique significantly influences the surface properties, durability, stability and in turn the degradation rate of the coating

The effect of sintering temperature plays an important role in forming HA in forming HA crystals [3, 42]. The fact the peak dimension of HA powders is narrower shows that the crystallized level of HA dust increases. It is seen that there is HA peak

Elemental calcium and phosphorus were also detected on the rinsed and dried electrode surface by our EDX measurements. We therefore speculate that a deposited calcium phosphate layer existed on the electrode surface, which inhibited the electrochemical reaction and increased the  $R_p$  by covering the electrode surface and blocking the mass transportation of oxygen and/or reaction products to and/or from the electrode surface.

### 3.4. FTIR Spectroscopy

In these spectra it is relatively easy to observe the following absorption bands characteristic of HAP.

Bands of OH<sup>-</sup> group are seen 3750, 630, 335 cm<sup>-1</sup> in HA structure. The characteristics bands of phosphate compounds are seen 900–1200, 563–601 cm<sup>-1</sup>. Ca–PO<sub>4</sub> are seen 275, 295 cm<sup>-1</sup> band ve Ca–OH are seen 335 cm<sup>-1</sup> band. PO<sub>4</sub><sup>3-</sup> groups are observed in the 1090, 14–962, 18–601, 41–473, 82–569, 21 cm<sup>-1</sup> bands region, which are characteristic of HAP [29, 42–44].

#### 4. RESULTS

1. As a result, HAP coatings have provided over 82.9% pure Ti and its corrosion in Ti6Al4V alloy has 89.49% and over inhibition. 96.5% inhibition in the front surface proceeded sample plated HAP has been provided for 316L stainless steel in Ringer solution.

2. All front surface processes are effective on monitoring corrosion and clinging HAP coating to the surface. And anodic front surface process is effective on 316L steel in Ringer medium and HNO<sub>3</sub> and BA front surface process is effective in NaCl medium.

3. It has been seen that the impedance values have increased in HAP coatings (Ti and Ti6Al4V). HAP coatings have raised the resistance of the metals.

4. Warburg impedance in outer porous layer is related to diffusion process in devre model for Ti and Ti6Al4V. This shows that there have been two parts, i.e. inner barrier layer and outer porous layer, on Ti and Ti6Al4V surfaces plated HAP.

5. The values of polarization resistance in the samples plated HAP for 316L steel has increased in 0.9% NaCl and Ringer solutions.

6. It is seen clearly in SEM images that there are open pores and attachments among pores in the coating. It is important to use HAP structure preferably for the cells producing bones, because the structure of HAP is rough and porous morphologically. Because pretreatment surface processes have corroded the surface of the metals, it provided better clinging of HAP coatings to the surface.

7. It is observed in EDX analyses of the samples plated HAP that there is only Ca, O, and P on the surface. Ca/P ratio varies in 1.36–2.00 level. As Ca/P ratio increases, the inhibition increases too.

8. It is seen in XRD images of HAP powder that there are the structures of rutil, HA and calcium phosphate.

9. It is observed in FTIR analysis that HA absorption bands are seen all sintered powders.

10. If corrosion potentials are in mixture, it has shifted to both cathodic and anodic potentials. Therefore HAP coatings have showed mixed inhibitor effect.

#### ACKNOWLEDGMENTS

The authors acknowledge the financial support of TUBITAK (Project no. 107M563).

#### REFERENCES

- Balamurugan, A., Balossier, G., Kannan, S., and Rajeswari, S., *Mater. Lett.*, 2006, vol. 60, p. 2288.
- Gan, L. and Pilliar, R., *Biomaterials*, 2004, vol. 25, p. 5303.
- Metikos-Hukovic, M., Tkalcec, E., Kwokal, A., and Piljac, J., *Surface and Coatings Technology*, 2003, vol. 165, p. 40.
- Kannan, S., Balamurugan, A., and Rajeswari, S., *Mater. Lett.*, 2003, vol. 57, p. 2382.
- Kannan, S., Balamurugan, A., and Rajeswari, S., *Electrochim. Acta*, 2004, vol. 49, p. 2395.
- Kannan, S., Balamurugan, A., and Rajaeswari, S., *Electrochim. Acta*, 2005, vol. 50, p. 2065.
- Kannan, S., Lemos, I.A.F., Rocha, J.H.G., and Ferreira, J.M.F., *J. Solid State Chemistry*, 2005, vol. 178, p. 3190.
- Krupa, D., Baszkiewicz, J., Kozubowski, J.A., et al., *Biomaterials*, 2001, vol. 22, p. 2139.
- Krupa, D., Baszkiewicz, J., Kozubowski, J.A., et al., *J. Materials Processing Technology*, 2003, vol. 144, p. 158.
- Krupa, D., Baszkiewicz, J., Rajcel, B., et al., *Vacuum*, 2005, vol. 78, p. 161.
- Krupa, D., Baszkiewicz, J., Rajcel, B., et al., *Vacuum*, 2007, vol. 81, p. 1310.
- Xu, W., Hu, W., Li, M., and Wen, C., *Mater. Lett.*, 2006, vol. 60, p. 157.
- Wang, D., Chen, C., Liu, X., and Lei, T., *Colloids and Surfaces B: Biointerfaces*, 2007, vol. 57, p. 237.
- Grandfield, K. and Zhitomirsky, I., *Materials Characterization*, 2008, vol. 59, p. 61.
- Guo, L. and Li, H., *Surface and Coatings Technology*, 2004, vol. 185, p. 268.
- Jalota, S., Bhadur, S.B., and Tas, A.C., *Materials Science and Engineering*, 2007, vol. 27, p. 432.
- Jonasova, L., Müller, F.A., and Helebrant, A., *Biomaterials*, 2004, vol. 25, p. 1187.
- Narayanan, R., Dutta, S., and Seshadri, S.K., *Surface and Coatings Technology*, 2006, vol. 200, p. 4720.
- Kutty, T.R.N., *Indian J. Chem.*, 1973, vol. 11, p. 695.
- Skinner, H.C.W., Kittelberger, J.S., and Beebe, R.A., *J. Phys. Chem.*, 1975, vol. 74, p. 2017.
- Kijima, T. and Tsutsumi, M., *J. Am. Ceram. Soc.*, 1979, vol. 62, p. 455.
- Wang, P.E. and Chaki, T.K., *J. Mater. Sci. Mater. Med.*, 1993, vol. 4, p. 150.
- Ducheyne, P., Radin, S., Heughebaert, M., and Heughebaert, J.C., *Biomaterials*, 1990, vol. 11, p. 244.
- Sridhar, T.M., Kamachi Mudali, U., and Subbaiyan, M., *Corrosion Sci.*, 2003, vol. 45, p. 2337.
- Balamurugan, A., Balossier, G., Kannan, S., et al., *Materials Science and Engineering*, 2007, vol. 27, p. 162.
- Engin, N.O., and Tas, A.C., *Bioceramics J. Am. Ceram. Soc.*, 2000, vol. 83, p. 1581.
- Giavaresi, G., Fini, M.A., Cigada, R., et al., *Biomaterials*, 2003, vol. 24, p. 158.
- Fini, M., Giavaresi, G., Greggi, T., et al., *J. Biomed. Mater. Res. A*, 2003, vol. 66, p. 176.

29. Baker, K.C., Anderson, M.A., Oehlke, S.A., et al., *Materials Science and Engineering*, 2006, vol. 26, p. 1351.
30. Zhang, S., Xianting, Z., Yongsheng, W., et al., *Surface-Coatings Technology*, 2006, vol. 200, p. 635.0
31. Gan, L. and Pilliar, R., *Biomaterials*, 2004, vol. 25, p. 5313.
32. Harle, J., Kim, H.W., Mordan, N., et al., *Acta Biomaterialia*, 2006, vol. 2, p. 547.
33. Moseke, C. and Gbureck, U., *Acta Biomaterialia*, 2010, vol. 6, p. 3815.
34. Dorozhkin, S.V., *Acta Biomaterialia*, 2010, vol. 6, p. 715.
35. Dorozhkin, S.V., *Biomaterials*, 2010, vol. 31, p. 465.
36. Bastidas, D.M., La Iglesia, V.M., Criado, M., et al., *Construction and Building Materials*, 2010, vol. 24, p. 2646.
37. Bohner, M., *Int. J. Care Injured*, 2000, vol. 31, p. S-D37.
38. Habraken, W.J.E.M., Wolke, J.G.C., and Jansen, J.A., *Advanced Drug Delivery Reviews*, 2007, vol. 59, p. 234.
39. Xiaoliang Cheng and Sharon G. Roscoe, *Biomaterials*, 2005, vol. 26, p. 7350.
40. Olefjord, I. and Elfstrom, B.O., *Corrosion*, 1982, vol. 38, p. 46.
41. Revesz, A.G. and Kruger, J., *Passivity of Metals, Corrosion Monograph Series*, Kruger, J., Ed., Princeton: Electrochemical Society, 1978, p. 137.
42. Eshtiagh-Hosseini, H., Housaindokht, M.R., and Chahkandi, M., *Mater. Chem. and Phys.*, 2007, vol. 106, p. 310.
43. Bogdanoviciene, I., Beganskiene, A., Tonsuaadu, K., et al., *Materials Research Bulletin*, 2006, vol. 41, p. 1754.
44. Balamurugan, A., Balossier, G., Kannan, S., and Rajeswari, S., *Mater. Lett.*, 2006, vol. 60, p. 2288.